Journal of Instrumentation

PAPER • **OPEN ACCESS**

Design and simulation of modified 3D-trench electrode sensors

Jinst

Published by IOP Publishing for Sissa Medialab

Received: *September 26, 2023*
Accepted: *October 26, 2023*
Published: *November 29, 2023*

24th International Workshop on Radiation Imaging Detectors
Oslo, Norway
25–29 June 2023

Design and simulation of modified 3D-trench electrode sensors

Jixing Ye,[a,b,*] **Angelo Loi,**[c] **Adriano Lai**[c] **and Gian-Franco Dalla Betta**[a,b]

[a] *Dipartimento di Ingegneria Industriale, Università degli Studi di Trento, Via Sommarive 9, 38123 Trento, Italy*
[b] *Trento Institute for Fundamental Physics and Applications-Istituto Nazionale di Fisica Nucleare (TIFPA-INFN), Via Sommarive 14, 38123 Trento, Italy*
[c] *Istituto Nazionale Fisica Nucleare, Sezione di Cagliari, Cittadella Universitaria, SP Monserrato-Sestu km 0.7, 09042 Monserrato (CA), Italy*

E-mail: jixing.ye@unitn.it

Abstract: Future experiments at high-luminosity hadron colliders will involve unprecedent levels of pile up, calling for ultrafast detectors in order to add time information to distinguish between particle tracks. The unique geometry of 3D sensors enables to achieve very good timing performance, with the additional benefit of high radiation hardness. Remarkable results in terms of temporal resolution have been reported for 3D sensors with columnar electrodes (~30 ps) and even better with trenched electrodes (~10 ps), because of a more uniform distribution of the electric field and weighting field. However, 3D-trench technology is more complex, and has still to be optimized in terms of both fabrication process and pixel layout. To this purpose, as an alternative to the existing design which features continuous (p^+) ohmic trenches, we propose a new variant by introducing a gap (~10 µm) in the p^+ trenches and placed offset with respect to the readout (n^+) trenches, so as to reduce the risk of lithographical defects that were observed in mm's long ohmic trenches, thus improving the fabrication yield.

TCAD simulations confirmed that the impact of the gap on the uniformity of the electric and weighting field is minimum, and good charge collection efficiency performance is preserved up to large fluences. Further Monte Carlo time-resolved simulations are performed on both the standard and modified geometries showing comparable temporal resolutions.

Keywords: Detector modelling and simulations II (electric fields, charge transport, multiplication and induction, pulse formation, electron emission, etc); Hybrid detectors; Solid state detectors; Timing detectors

*Corresponding author.

https://doi.org/10.1088/1748-0221/18/11/C11021

2023 JINST 18 C11021

Contents

2023 JINST 18 C11021

1 Introduction

The projected upgrade of the Large Hadron Collider (LHC) to the High Luminosity LHC (HL-LHC) brings about the question of the era beyond the HL-LHC, which is the Future Circular Collider (FCC). The foreseen integrated luminosity in such experiments (e.g. FCC-hh) is at least 5 times larger than that of the HL-LHC, with event pile-up of 1000 per bunch crossing [1]. The large number of event pile-up requires both low occupancy (<1%) to reduce the probability of two particles hitting the same pixel simultaneously, and a temporal resolution of the order of tens of picosecond at the same time in order to disentangle different events for precise vertexing [2, 3]. Meanwhile, the associated extreme radiation level ($\sim 1 \times 10^{17} n_{\mathrm{eq}}/\mathrm{cm}^2$ per year) necessitates detectors with strong radiation hardness. To cope with these stringent requirements, the FCC calls for dedicated detecting systems capable of 4D tracking, and withstanding extreme level of radiation damages. Significant efforts on the R&D of 4D tracking detectors have led to the emergence of very appealing candidates featuring different flavours of detectors, such as Ultra-Fast Silicon Detector (UFSD) and 3D detectors.

State-of-the-art UFSD prototypes, incorporating carbon implant and trench isolation, suggested a temporal resolution of ~30 ps after fluence up to $\sim 3.5 \times 10^{15} n_{\mathrm{eq}}/\mathrm{cm}^2$, but the resistance to higher fluences has yet to be demonstrated [4].

Different from planar detectors that have shallow electrodes sitting on the surfaces of the wafer, 3D detectors feature electrodes that penetrate deep into the substrate, which decouples the inter-electrode distance with the bulk width. Therefore, drift distance can be made smaller in order to provide strong radiation hardness and high temporal resolution [5]. The first property has so far been mostly exploited, recently leading to a new generation of small-pitch pixel sensors to be applied at the HL-LHC, e.g., in the innermost tracking layer of the ATLAS detector [6].

A columnar 3D single-pixel test structure of $50 \times 50\,\mu m^2$ geometry, fabricated at CNM (Barcelona, Spain), was tested using a fast discrete readout channel, showing a temporal resolution of ~30 ps at 150 V bias and −20 °C [7]. Moreover, to face the non-uniform electric field and weighting field caused by the columnar electrode in the small pitch design, the idea of 3D detectors with trench electrodes was initially brought up by S. Parker [8] and later developed within the INFN TimeSPOT Project [9]. Comprehensive simulations and measurements show that 3D-trench electrode sensors can provide a temporal resolution of ~ 10 ps both before and after irradiation up to $2.5 \times 10^{16} n_{eq}/cm^2$, also proving the excellent radiation hardness of the design [10–12].

The outstanding performance of 3D-trench electrode sensors is achieved at the expense of a more complex fabrication technology, that is yet to be optimized. In particular, lithographical defects were observed in continuous ohmic trench electrodes, whose length extends to the full sensor size, raising concerns about the fabrication of long ohmic trench electrodes, which could range up to more than 1 cm in large size pixel sensors.

In this paper, we propose a new layout variant by introducing a gap in the ohmic electrode, and placing it offset with respect to the junction electrode, so as to ease the fabrication complexity and minimize the influence introduced by the gap. TCAD simulations show that distorted electric field as well as weighting field, exist only in the vicinity of the gap. Further Monte Carlo simulations carried out prove that the temporal resolution of the new design is comparable.

2 Simulation approach

2.1 Device description

3D-trench electrode detectors are fabricated at FBK using the single-sided technology developed for small-pitch 3D pixels [13], with stepper lithography to improve the definition of layout details and increase the fabrication yield [14]. A thin sensor wafer (150 µm) is directly bonded to a highly doped handle wafer, so that mechanical stability can be assured. The cross section of the device is shown in figure 1 (left). All the electrodes are etched from the front side: the ohmic electrodes penetrate the entire sensor wafer into the handle wafer for straightforward biasing, while the junction electrodes are kept at a safe distance from the handle wafer (gap = 15 µm) to avoid early breakdown. The p-spray layer on the front side ensures the isolation between different pixels after surface damage. Thinning of the handle wafer is needed as a post-processing in order to meet the material budget, followed by coating of a metal layer as a final step.

The feasibility of this technology has been demonstrated within the INFN TimeSPOT project, with excellent results in terms of temporal resolution and radiation hardness. However, lithographical defects were observed in the mm long ohmic trenches, with impact on the fabrication yield. To address this challenge, a 10 µm gap is introduced in the ohmic trench electrode. Figure 1 (right) shows the layouts of the existing 3D-trench electrode sensor and the modified design. The gap is made reasonably short and placed offset with respect to the junction electrode to minimize the region with distorted fields (e.g. electric field, weighting field).

2023 JINST 18 C11021

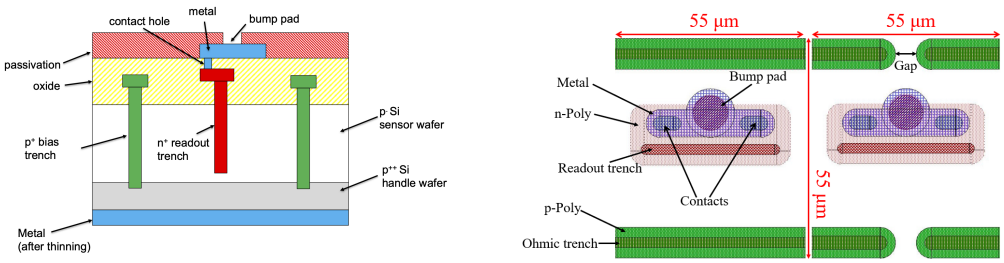

Figure 1. Schematic cross-section (left) and pixel layout (right) of 3D-trench sensors.

2.2 TCAD simulation

Key aspects, such as the charge collection efficiency (CCE) and the signal dynamics predominantly depend on the electric field distribution in the active bulk. Therefore, an in-depth study of the electric field in the bulk region is necessary and can be achieved using 2D domains, due to the fact that the charges in 3D detectors are collected laterally. Figure 2 shows the simulation domain of the two designs. TCAD simulations are performed on Synopsys Sentaurus, incorporating typical models such as doping dependent Shockley-Read-Hall generation/recombination, high field saturation, etc [15]. While most of the models used the default values, the minority carrier lifetimes of 1 ms were chosen, which represent the typical values of the FBK technology.

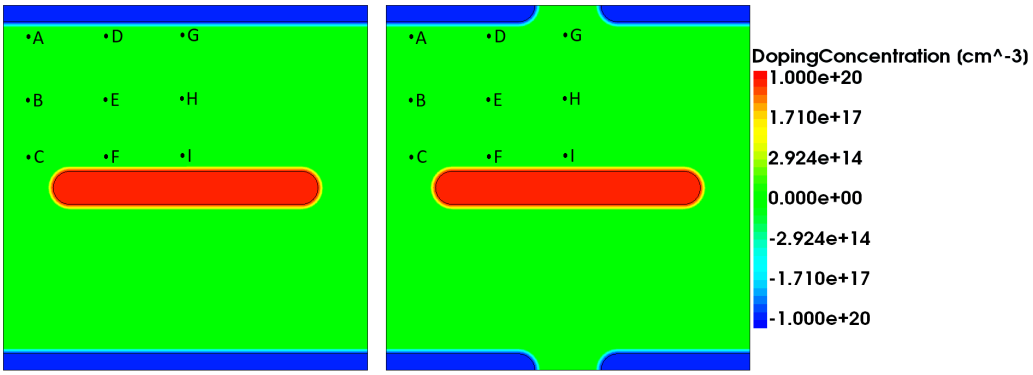

Figure 2. Simulation domain of the 3D-trench pixel sensor (left) and the 3D dashed-trench pixel sensor (right).

Besides static simulations, transient simulations based on the HeavyIon model are also performed to evaluate the signal efficiency (SE). Well-defined meshes along the track of the impinging particle as well as small enough time steps are necessary ingredients for an accurate description of the charge collection process, which made a scanning of the entire pixel impossible in terms of simulation time. Therefore, positions representative of the critical regions are chosen for the transient simulation, as indicated by the black dots in figure 2. Furthermore, the CERN bulk damage model is used to assess the signal efficiency of the two designs after bulk damage [16]

2.3 Monte Carlo simulation

AllPix^2 is a powerful simulation framework able to simulate the charge transport in the detector and the digitization process in the front-end electronics [17, 18]. The framework uses *Geant*4 for the estimation of energy deposition in the active volume; electric field and weighting potential maps,

2023 JINST 18 C11021

calculated from TCAD simulations, are then imported for the propagation of the charges and the calculation of the induced signal, respectively; dedicated front-end electronics can be emulated and used at last for signal digitization by providing associated parameters such as the feedback capacitance, the rise time constant, etc.

In this work, we evaluated the temporal resolution of the central pixel of a 3×3 array using minimum ionizing particles (MIP). The Jacoboni-Canali model is used for the propagation of the charges; the front-end simulation module (e.g. *CSADigitizer*) is used to derive the time-of-arrival (ToA) with a configurable time-to-digital converter (TDC) [18]. Here we used the *DefaultDigitizer* as the front-end module and the ToA is extracted as the time when the integrated input charge crosses the threshold, which is set to 1000e.

3 Simulation results

3.1 Field maps

Figure 3 shows the electric field of the two 3D-trench electrode designs at bias voltage $V_b = 100$ V. It can be seen that the 3D-trench electrode sensor has uniformly high electric field in almost the entire pixel area, with small spots of low electric field only in-between the junction electrodes. Similarly, the electric field is high in most of the region in the new variant, but relatively low electric field regions also exist in the vicinity of the introduced gap.

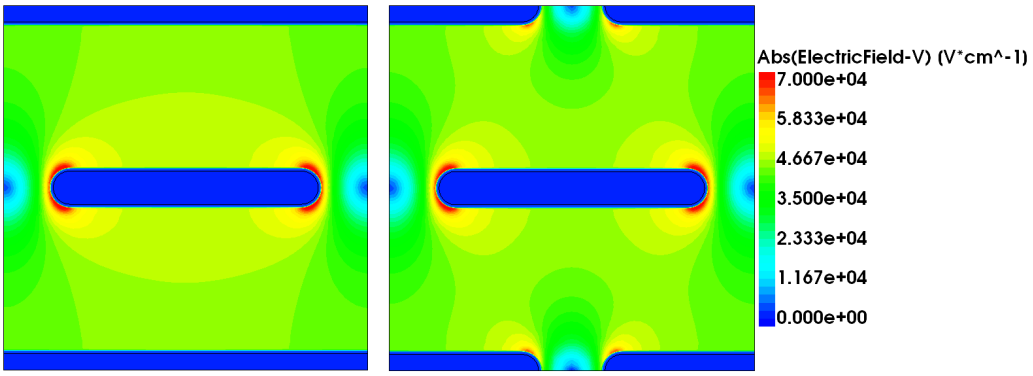

Figure 3. Electric field of the 3D-trench electrode sensor (left) and the 3D dashed-trench electrode sensor (right) at bias voltage $V_b = 100$ V.

The fraction of the charges induced on each electrode depends on the weighting potential, which is solely subjected to the geometry of the electrodes. Figure 4 shows the weighting potential of the two designs: a 3×3 array is used for the simulation in order to properly define the boundary conditions. As can be seen, the weighting potential is only limited to the two lateral neighboring pixels in the existing design, due to the shielding effect of the ohmic electrodes. The situation does not change much in the new variant, with negligible weighting potential extending to the gap region. These very similar distributions are reflected also in the maps of hole and electron drift velocities (not shown), which feature saturated values in most of the pixel area in both designs.

2023 JINST 18 C11021

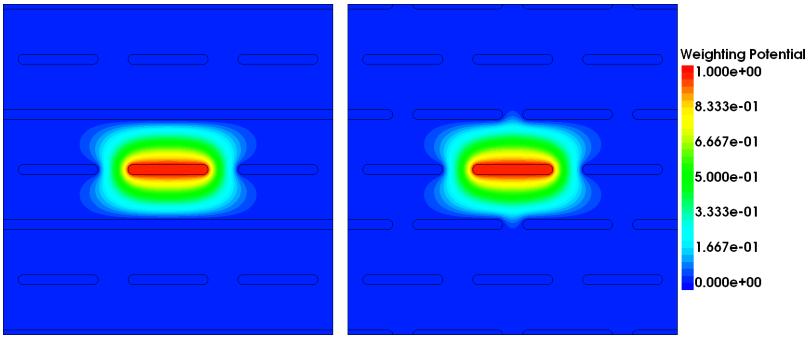

Figure 4. Weighting potential of the 3D-trench electrode sensor (left) and the 3D dashed-trench electrode sensor (right).

3.2 Induced current

The induced current of a single element charge (q) at arbitrary positions is determined by the weighting field (E_w) and the charge drift velocity (V_d), which in turn depends on the electric field. This can be expressed by the Shockley-Ramo's theorem: $i = -qE_w \cdot V_d$.

Figure 5 shows the calculated Ramo maps of holes (top) and electrons (bottom) when the reverse bias is 100 V. We can see that both hole and electron induced current in the two designs are almost identical, except for the gap region.

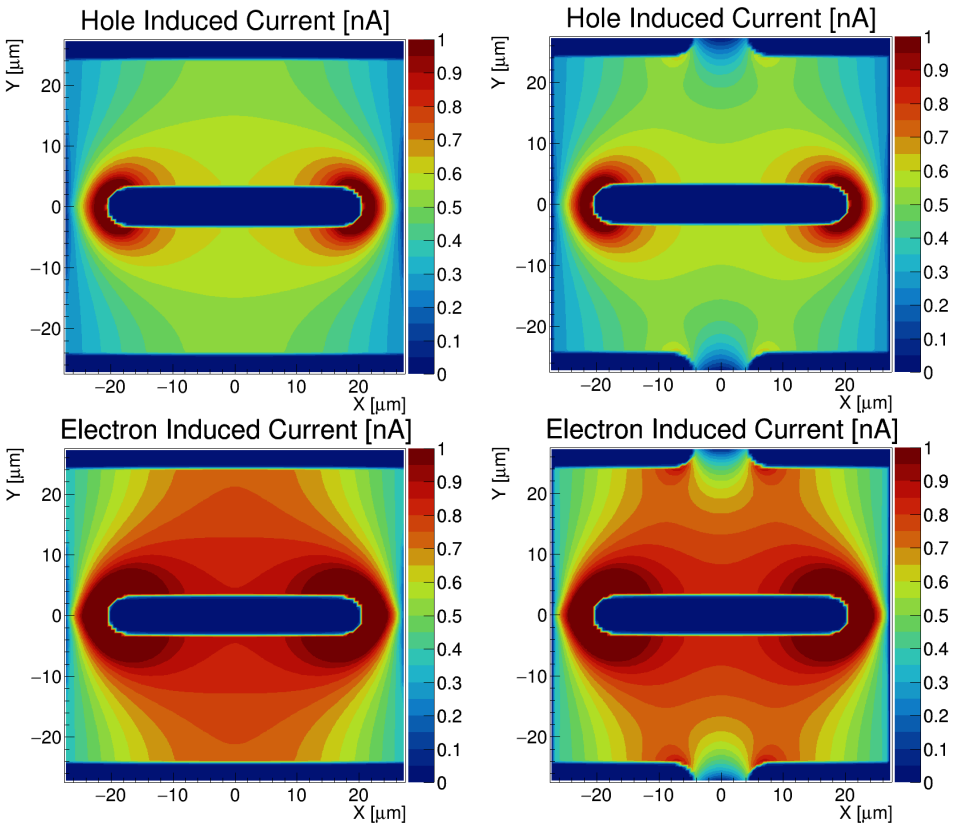

Figure 5. The top row shows the hole induced current of the 3D-trench electrode sensor (left) and the 3D dashed-trench electrode sensor (right) at bias voltage V_b = 100 V, the electron induced current is shown in the bottom row.

2023 JINST 18 C11021

3.3 Signal efficiency

The impact of the gap on the radiation hardness has been evaluated by TCAD transient simulations using the HeavyIon model; the CERN model is used for the simulation of bulk damages effects. The results of static simulations (electric field map, charge drift velocity map, etc) are imported as an input for the transient simulation. The nine MIP impinging positions shown in figure 2 and different radiation fluences, up to $2 \times 10^{16} n_{\mathrm{eq}}/\mathrm{cm}^2$, were chosen for the simulations. In all conditions, the signal efficiency (SE) was calculated as the ratio of the collected charge after irradiation and before irradiation.

Negligible differences (at most 2%) are observed in the SE of the two designs for positions A–F. After the largest fluence of $2 \times 10^{16} n_{\mathrm{eq}}/\mathrm{cm}^2$, the SE at 140 V bias is still remarkably good:80% (A), 73% (B), 41% (C), 79% (D), 70% (E), and 38% (F). On the contrary, some differences in the SE are observed for positions G–I, as illustrated in figure 6. As expected, the largest deviation, ∼10%, is for position G, the closest to the gap, whereas results for the worst case (position I) are very similar, and still larger than 35% at 140 V after the largest fluence.

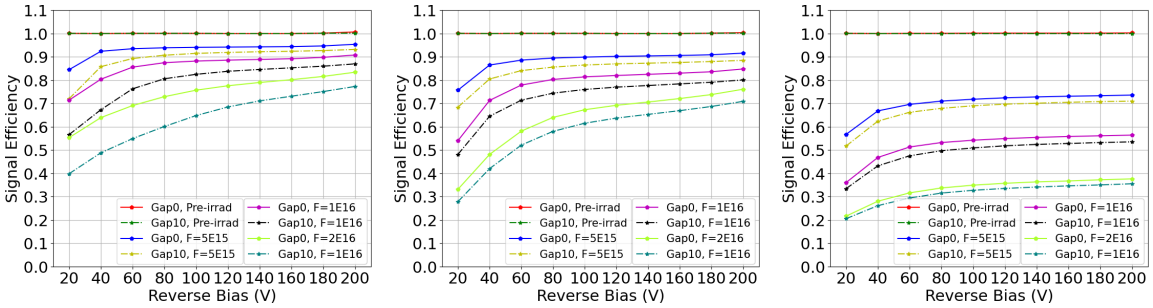

Figure 6. Signal efficiency for impinging positions G (left), H (centre), and I (right), as a function of bias voltage and at different fluences in the 3D-trench electrode sensor (solid lines) and the new design variant (dashed lines).

3.4 Monte Carlo simulations

Thanks to the AllPix^2 framework, it is possible to perform end-to-end MonteCarlo simulations, which provide an insight into the performance of the whole detecting system. It is worth mentioning that we scanned one quarter of the pixels for both structures, and the results are representative enough due to symmetry. Figure 7 (left) shows the ToA map of the existing design: the yellow regions on the top and bottom of the plots correspond to the electrodes, and they are filtered out when calculating the mean ToA and the associated standard deviation. We can see that the sensor has a small standard deviation, around 11 ps and this result is within the expectation for non-irradiated 3D-trench electrode sensors [12]. Moreover, the ToA is uniform in most parts of the pixel, with higher values observed near the edge of the pixel. Similar results are obtained from the new variant, as shown on figure 7 (right). The calculated mean ToA and the standard deviation used the same filtering method, and we can see the two designs have comparable temporal resolutions.

2023 JINST 18 C11021

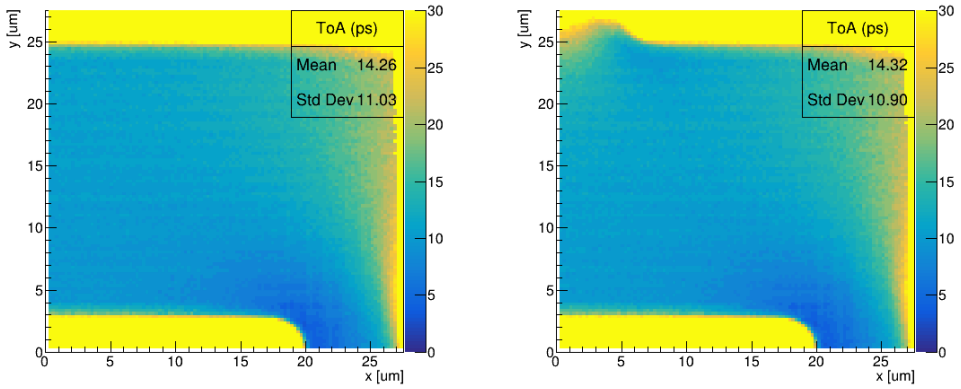

Figure 7. ToA of the 3D-trench electrode sensor (left) and the 3D dashed-trench electrode sensor (right) at bias voltage $V_b = 100$ V.

4 Conclusions

3D-trench electrode sensors are promising candidates for future experiments because of their excellent radiation hardness and temporal resolution. In order to improve the fabrication yield of large (~cm^2) sensors, we have proposed a modified pixel layout with dashed-ohmic-electrode geometry, and validated the design by TCAD and Monte Carlo simulations in comparison with the existing design.

TCAD static simulations show a uniform distribution of the electric field in most regions of the pixel, except for the vicinity of the introduced gap. The same situation has been observed in the calculated Ramo map. TCAD transient simulations based on the HeavyIon model and incorporating bulk damage effects suggest identical signal efficiencies in regions far away from the gap, whereas the signal efficiency is slightly lower in the small region affected by the gap, but its values are still remarkably good. Monte Carlo simulations show a comparable temporal resolution of ~ 11 ps in both designs, a result that is in good agreement with the values measured on existing samples of the standard design. The considered designs have been implemented in a fabrication batch currently under way at FBK in the framework of the AIDAInnova Project.

Acknowledgments

The authors acknowledge funding from INFN-CSN5 with Project TimeSPOT, and the European Union's Horizon 2020 Research and Innovation programme under GA no. 101004761. The authors would also like to warmly thank Simon Spannagel for his help with the AllPix^2 simulations and fruitful discussions.

References

[1] FCC collaboration, *FCC-hh: The Hadron Collider: Future Circular Collider Conceptual Design Report Volume 3*, *Eur. Phys. J. ST* **228** (2019) 755.

[2] N. Cartiglia et al., *4D tracking: present status and perspectives*, *Nucl. Instrum. Meth. A* **1040** (2022) 167228 [arXiv:2204.06536].

2023 JINST 18 C11021

[3] TIMESPOT collaboration, *A System Approach towards Future Trackers at High Luminosity Colliders: the TIMESPOT Project*, in the proceedings of the *2018 IEEE Nuclear Science Symposium and Medical Imaging Conference*, Sydney, NSW, Australia (2018), p. 1–3 [DOI:10.1109/NSSMIC.2018.8824310].

[4] R. Arcidiacono et al., *State-of-the-art and evolution of UFSD sensors design at FBK*, *Nucl. Instrum. Meth. A* **978** (2020) 164375.

[5] S.I. Parker, C.J. Kenney and J. Segal, *3D — A New architecture for solid state radiation detectors*, *Nucl. Instrum. Meth. A* **395** (1997) 328.

[6] S. Terzo et al., *Novel 3D Pixel Sensors for the Upgrade of the ATLAS Inner Tracker*, *Front. Phys.* **9** (2021) 2.

[7] G. Kramberger et al., *Timing performance of small cell 3D silicon detectors*, *Nucl. Instrum. Meth. A* **934** (2019) 26 [arXiv:1901.02538].

[8] S. Parker et al., *Increased speed: 3D silicon sensors. Fast current amplifiers*, *IEEE Trans. Nucl. Sci.* **58** (2011) 404.

[9] R. Mendicino et al., *3D trenched-electrode sensors for charged particle tracking and timing*, *Nucl. Instrum. Meth. A* **927** (2019) 24.

[10] L. Anderlini et al., *Intrinsic time resolution of 3D-trench silicon pixels for charged particle detection*, 2020 *JINST* **15** P09029 [arXiv:2004.10881].

[11] D. Brundu et al., *Accurate modelling of 3D-trench silicon sensor with enhanced timing performance and comparison with test beam measurements*, 2021 *JINST* **16** P09028 [arXiv:2106.08191].

[12] A. Lampis et al., *10 ps timing with highly irradiated 3D trench silicon pixel sensors*, 2023 *JINST* **18** C01051 [arXiv:2209.14632].

[13] D.M.S. Sultan et al., *First Production of New Thin 3D Sensors for HL-LHC at FBK*, 2017 *JINST* **12** C01022 [arXiv:1612.00638].

[14] M. Boscardin et al., *Advances in 3D Sensor Technology by Using Stepper Lithography*, *Front. Phys.* **8** (2021) 647.

[15] Synopsys Inc., *Sentaurus Device User Guide Version R-2020.09*, San Jose, CA, U.S.A., September 2020.

[16] Å. Folkestäd et al., *Development of a silicon bulk radiation damage model for Sentaurus TCAD*, *Nucl. Instrum. Meth. A* **874** (2017) 94.

[17] S. Spannagel and P. Schütze, *Allpix^2 — silicon detector Monte Carlo simulations for particle physics and beyond*, 2022 *JINST* **17** C09024 [arXiv:2112.08642].

[18] S. Spannagel et al., *Allpix^2: A Modular Simulation Framework for Silicon Detectors*, *Nucl. Instrum. Meth. A* **901** (2018) 164 [arXiv:1806.05813].

2023 JINST 18 C11021